Published in final edited form as:
J Vis. ; 8(11): 9.1–9.8. doi:10.1167/8.11.9.

A 'dipper' function for texture discrimination based on orientation variance

Michael Morgan,
Department of Optometry, City University London, UK

Charles Chubb, and
Department of Cognitive Sciences, University of California, Irvine, USA

Joshua A. Solomon
Department of Optometry, City University London, UK

Abstract

We measured the just-noticeable difference (JND) in orientation variance between two textures (Figure 1) as we varied the baseline (pedestal) variance present in both textures. JND's first fell as pedestal variance increased and then rose, producing a 'dipper' function similar to those previously reported for contrast, blur, and orientation-contrast discriminations. A dipper function (both facilitation and masking) is predicted on purely statistical grounds by a noisy variance-discrimination mechanism. However, for two out of three observers, the dipper function was significantly better fit when the mechanism was made incapable of discriminating between small sample variances. We speculate that a threshold nonlinearity like this prevents the visual system from including its intrinsic noise in texture representations and suggest that similar thresholds prevent the visibility of other artifacts that sensory coding would otherwise introduce, such as blur.

Keywords

visual acuity; computational modeling; learning; middle vision; texture

Introduction

The nervous system is noisy and all sensory signals are subject to perturbation (Barlow, 1981). Studies of orientation classification (Dakin, 1999; Dakin & Watt, 1997; Morgan, 1990) suggest that the visual system perturbs the orientations of individual elements with a variance of approximately 1 deg. There is a problem, then, in understanding why we do not see orientation variance in a texture composed of parallel elements, like that on the left-hand side of Figure 1. If the internally represented orientation of each element were independently sampled from a Gaussian distribution, then all the elements should look different, even if

Corresponding author: Michael Morgan. m.morgan@city.ac.uk. Address: Department of Optometry, City University London, Northampton Square, London, EC1V 0HB, UK.

Commercial relationships: none.

Europe PMC Funders Author Manuscripts

they are physically parallel. In an array of 121 elements (Figure 1) it would not be at all unlikely that a particular element would have an apparent orientation 2σ from its true value. A possible resolution of this paradox is that when we see a texture as uniform, we are not seeing the orientation of every element in the texture, but rather the output of a specialized mechanism that computes orientation variance. If stimulation of this mechanism were subject to a threshold nonlinearity, then the perceived uniformity of a uniform texture could be explained.

A threshold would be useful for eliminating early noise from mid-level visual representations. The idea that sensory systems discount their own imperfections is suggested by the absence of sensory hallucinations in everyday life, and from the apparent sharpness of the retinal image. In reality, the retinal image is considerably blurred by imperfections in the optics, and by inescapable diffraction through a small pupil, but we become conscious of this blur only when it exceeds normal levels, for example, when we need spectacles. The idea that blur is detected only when it exceeds a threshold is supported by studies of blur discrimination, both in stationary (Georgeson, 1994; Watt & Morgan, 1983) and in moving images (Burr, 1980, 1981; Burr & Morgan, 1997; Morgan & Benton, 1989; Paakkonen & Morgan, 1993). Blur discrimination thresholds between two patterns have a characteristic ‘dipper’ shape similar to that for contrast discrimination (Nachmias & Sansbury, 1974). As small amounts of blur are added to both images, the just-noticeable difference (JND) in blur first falls, and then rises again. The initial fall would be expected from a threshold, since a small amount of blur would raise the response of the mechanism to just below the threshold, making an additional increment easier to see. The rise in JND at even higher pedestal levels, referred to as ‘masking’, is usually explained by a compressive nonlinearity (Foley, 1994; Legge & Foley, 1980; Ross, Speed, & Morgan, 1993), or alternatively by multiplicative sensory noise (Solomon, 2007).

In this investigation we sought evidence for a similar dipper in the case of orientation variance discrimination. There were already indications of such an effect in the literature. Motoyoshi and Nishida (2001) measured the JND’s between two different levels of orientation contrast in bimodal orientation textures. Although they were mainly interested in the masking region, where JND’s increased with the pedestal contrast, Motoyoshi and Nishida also noted facilitation at small, nonzero pedestal contrasts. That is, they found that JND’s formed a dipper function of pedestal contrast.

Facilitation at small, nonzero *luminance* contrasts is normally taken as evidence for a threshold nonlinearity (e.g., Foley & Legge, 1981; Legge & Foley, 1980). However, in the case of variance discrimination, facilitation is expected simply on the basis of intrinsic noise (Laming, 1986; Paakkonen & Morgan, 1993).[1] The full derivation is given in the Appendix A, but the informal argument runs thus. Suppose, in a 2AFC experiment, the observer compares two sample variances, each of which reflects the visual system’s internal noise as well as the stimulus variance. The function mapping stimulus variance to sample variance

[1]Paakkonen and Morgan (1993) assumed that two blurred edges were discriminated as a function of the difference in their internally represented blur, which combined extrinsic and intrinsic blur by convolution (Equation 6 of their paper). However, they assumed Weber’s Law rather than deriving it from sampling as we do in this paper.

will thus have two distinct parts; a flat part, in which the stimulus variance is negligible compared to the internal noise, and a steadily increasing part, in which the internal noise is negligible. Because of the flat part, any criterion increase in sample variance will require a larger increase in stimulus variance when sample variance is low.

The Appendix A shows that dipper functions are predicted even for an ideal observer who compares sample variances, whether or not there is an additional threshold nonlinearity. We wished to determine whether the addition of a sensory threshold would significantly improve the ideal observer's fit to variance discriminations.

Methods

In addition to the extensive observations undertaken by three experienced observers, a shorter series was completed by four psychophysically practiced observers who did not know the purpose of the experiment. Apart from noting that all of these observers showed facilitation (i.e. a 'dip'), we do not report the latter group's data further.

Stimuli were presented on the LCD screen of a Sony Vaio (PGC-TR5MP) laptop computer using MATLAB and the PsychToolbox (Brainard, 1997) for Windows. Screen size was 1280 × 768 pixels (230 × 140 mm). Only the Green LCD's were used, and the mean luminance was 56 cd/m^2. The viewing distance was approximately 57 cm so that the pixel size was approximately 0.018 deg of visual angle. The texture elements were Gabor wavelets of maximum contrast. Specifically, the Weber contrast g varied as a function of position x, y with respect to the center of the wavelet as follows:

$$g(x,y,\theta) = exp\left(-\frac{x_\theta^2+y_\theta^2}{2\sigma^2}\right) sin\left(2\pi\frac{x_\theta}{\lambda}\right) \quad (1)$$

where λ (the wavelength of the windowed grating) is 0.1198 deg, σ (the space constant of the window) is $\lambda/2$, and θ gives the angle normal to grating orientation; that is,

$$x_\theta = x\,cos(\theta) + y\,sin(\theta) \quad (2)$$

and

$$y_\theta = -x\,sin(\theta) + y\,cos(\theta) \quad (3)$$

The elements were laid out in an 11 × 11 lattice with spacing 3λ, slightly perturbed by displacing each elements randomly in x and y by an amount drawn from a uniform pdf with width 1.5λ. Thus, the whole array subtended approximately 3.6 deg of visual angle. The jitter was resampled between each of the two stimulus presentations on every trial.

On each trial two textures like those in Figure 1 were shown, each for 200 msec and with a 200-msec blank interval in between. Element orientations θ were drawn from Gaussian probability density functions. For one of the two textures, the density had random mean and "pedestal" variance σ_p^2. The density for the other texture had a different random mean and greater variance $(\sigma_p + \Delta\sigma)^2$. The mean orientation was randomized between presentations, to

prevent the use of any one orientation-tuned channel by the observer, and spatial position of the elements was jittered between presentations.

The QUEST procedure (Watson & Pelli, 1983) adaptively determined the JND $\Delta\sigma$ at which the observer was 82% correct. There was no feedback to indicate whether the response was correct or not. The pedestal variance was randomly selected on each trial from a set of preset values. A block of trials terminated when each of these preset values had been presented 50 times. Thus, when $\sigma_p \in \{0°, 1°, 2°, 4°, 8°, 16°\}$, as was the case for observers MM (6 blocks) and JAS (9 blocks) and IM (4 blocks), each block contained 300 trials. The four naive observers experienced only one block, with interleaved pedestal levels {0°, 1°, 2°, 4°} only.

Confidence limits (95%) for the JND were determined by exactly simulating the experiment 80 times with a bootstrapping procedure (Efron, 1982).

Results

Results (Figure 2) showed clear evidence for a 'dipper.' JND's were comparatively high when one of the patterns had no variance (the leftmost point on the graphs) and fell as variance was added. The curves in Figure 2 show the best fits to the data. (Note that these are not fits to the data points in the graph but are rather maximum likelihood fits (found with the FMINSEARCH function of MATLAB) of the model to data vectors consisting of the pedestal level, added signal level, and observer's response on every trial of the experiment.) These best-fitting parameter values and their associated log likelihoods are shown in Table 1.

A likelihood ratio test was used to compare the fits of the two models, one with and one without a threshold. Let L_C and L_U be the likelihoods of the best-fitting constrained and unconstrained models. As is well-known (e.g., Hoel, Port, & Stone, 1971), under the null hypothesis that the constrained model captures the true state of the world,

$$X = -2ln\left(\frac{L_C}{L_U}\right) \quad (4)$$

is asymptotically distributed as chi-square with 1 degree of freedom (for the single additional free parameter in L_U). The chi-square values were significant ($p < .010$) for observers MM and IM, but not for observer JAS. To give a more intuitive impression of the success of the two models, Figure 3 plots the relative likelihoods in comparison to two extreme baselines. The 'coin flipping' model has the simulated observer choose between the two intervals with equal probability, independently of the stimulus level or pedestal. This is as poor as a fit could be. The 'Weibull fits' model shows the best fit of a set of 2-parameter Weibull psychometric functions to the each of the pedestal conditions separately. This model has $2n$ free parameters, where n is the number of pedestals, in comparison to the 2 and 3 parameters of the models described in Table 1, and it is as good as a fit could be given the noise in the observer's data. It is satisfying to see that the models are much closer to the Weibull fits than to 'coin flipping'. The two versions of the intrinsic noise model, with and without an additional threshold, are seen to be very close.

Finally, to see if the threshold nonlinearity giving rise to the dipper was modifiable by experience, one observer (MM) undertook an extensive series of observations with a zero pedestal to see if performance would improve. Results (shown in Figure 4) failed to find any evidence for learning.

Discussion

We consider possible explanations for the dipper function found in our experiments.

Intrinsic noise

Intrinsic noise produces a dipper function for variance discrimination (see Appendix A). Both the initial fall and subsequent increase in JND (Weber's Law) arise because variance discrimination is necessarily a second-order computation. In a first-order computations, such as mean discriminations, intrinsic noise typically produces a flat region of the graph of JND vs. noise (e.g., Mansouri, Allen, Hess, Dakin, & Ehrt, 2004). On the other, hand, we expect, and find, a dipper function for contrast discrimination of orientation- and contrast-modulated gratings (Kingdom, Prins, & Hayes, 2003) and of dynamic visual noise (Morgan, McEwan, & Solomon, 2007). Blur discrimination is another clear case where there is a dipper (see Introduction) and where a case can be argued for its being a special case of variance discrimination in the luminance domain. The variance of point-luminance values across a sharp edge is different from that across less sharp edge; and indeed, Watt and Morgan (1983) produced their blurred edges by convolution of a step with a specified blurring function, defined by its variance.

Internal noise with a sensory threshold

Our results show qualitative agreement with the intrinsic noise model, but for all three observers the extent of facilitation is greater than predicted by the model. For two of the observers, the data were better fit by a model in which there is both internal noise and a threshold. The existence of a threshold could explain why we do not see the internal noise in a completely regular texture like that on the left of Figure 1. There are good reasons why the visual system should not represent its own noise when computing the variance of a pattern in the outside world, and there is collateral evidence that such thresholding happens in the case of blur, both of stationary and moving objects. The effect of the threshold will be to make textures appear slightly more regular than is in fact the case and this bias could be interpreted as a Bayesian prior in favor of seeing regularity in the world (Schwartz, Sejnowski, & Dayan, 2006). We admit, however, that this interpretation is entirely speculative, and that we do not have data that exclude other models.

Consistent with our current finding is previous work demonstrating an inability to extract local estimates of orientation from briefly glimpsed 'crowded' arrays when the regional orientation variance is small (Parkes, Lund, Angelluci, Solomon, & Morgan, 2001). Solomon, Felisberti, and Morgan (2004) noted this latter result implied that individual elements should appear more aligned than they really were and formulated a model wherein this 'smallangle assimilation' was the result of lateral amplification between neurons with the same orientation preference. (That model also contained a stronger, more broadly tuned,

Europe PMC Funders Author Manuscripts

lateral inhibition, which produced repulsion when orientation variance was larger.) Lateral amplification may underlie the sensory threshold manifest in our present results, but once again this is pure speculation. To make a stronger connection between small angle assimilation and the dipper function would require measurement of the dipper function in crowded displays.

Channel uncertainty

A different interpretation of the 'dipper' for contrast discrimination is that it reflects intrinsic uncertainty, which the observer has about the best channel to use when making the discrimination (Pelli, 1985). When the pedestal is zero, there are many channels the observer could monitor, each with a level of intrinsic noise. It is therefore likely that noise in one of the channels will masquerade as a signal. With a nonzero pedestal, however, the response in the channel most responsive to the signal will be elevated to a point where noise in other channels will be unlikely to exceed it. This model accounts well for many facts about contrast discrimination, but we find it difficult to see how it applies in the case of orientation variance discrimination. As far as orientation-tuned channels are concerned, the essence of our procedure was to ensure that the observer could not do the task by monitoring selected channels. Recall that the mean orientation of the stimuli was randomized both over trials and between the two stimuli in the 2AFC task. Thus, there was no information about variance to be derived from a single channel. The only way we can see to make an uncertainty model work is if there are different channels corresponding to different levels of variance. This is the possibility we consider next.

Multiple channel models of variance discrimination

Wavelength discrimination shows notches in certain regions of the spectrum, where there is a local minimum in the JND. The explanation is thought to be, in part, that these are regions where the difference in quantum catch of the L, M, and S cones is greatest as wavelength changes (Wyszecki & Stiles, 1967). It would be possible to envisage a similar model for variance discrimination, with one mechanism selectively but widely tuned to low variance, and another to a higher variance (Thompson, 1984). If there are such channels they should be revealed by selective adaptation.

Conclusion

The most parsimonious explanation of the dipper function for orientation variance is that it is produced by intrinsic noise in a specialized mechanism for variance computation. Our findings argue caution before automatically ascribing dippers, such as those for blur discrimination, to a threshold nonlinearity. However, we cannot rule out the possibility that there is an additional threshold, at least in two of our observers. Further investigations of the population are required to see whether there are genuine individual differences in this respect.

Acknowledgments

We would like to thank David Burr for encouragement, Marc Ernst for suggesting that intrinsic noise could masquerade as a sensory threshold, Beau Watson for remembering Paakkonen & Morgan, and Ahna Girshick for suggesting Figure 3 in her 2008 VSS talk. Supported by a Grant from the EPSRC.

Appendix A

Signal-detection theory for variance discrimination

Consider any 2AFC trial, in which the first alternative can be described as having the variance $(\sigma_p + \Delta\sigma)^2$ and the second alternative can be described as having the smaller variance σ_p^2. The model observer collects a sample of size $n + 1$ from the first interval, a sample of the same size from the second interval, and responds correctly when the variance of the former sample exceeds that of the latter. These two sample variances can be denoted by the independent random variables S and N, respectively. The expected response accuracy is given by the formula

$$\begin{aligned} P(C) = &\quad P(S>N) = \int_{-\infty}^{\infty} F_N(x)\, f_S(x)\, \mathrm{d}x \\ = &\quad \int_0^{\infty} F_N(x)\, f_S(x)\, \mathrm{d}x \end{aligned} \tag{A1}$$

where $F_N(x)$ is the cumulative distribution function (CDF) of N, and $f_S(x)$ is the probability density function (PDF) of S. The lower limit of integration is zero because neither S nor N can ever be negative.

Allowing internal noise

Consider what happens when each element of each sample is perturbed by internal Gaussian noise with zero mean and variance σ_{int}^2. In that case, S will be $\left[(\sigma_p+\Delta\sigma)^2+\sigma_{int}^2\right]/(n+1)$ times a chi-square random variable (call it U), having n degrees of freedom; and N will be $\left(\sigma_p^2+\sigma_{int}^2\right)/(n+1)$ times an independent chi-square random variable (call it V), also having n degrees of freedom; and probability correct is given by the formula

$$\begin{aligned} P(C) = &\quad P\left(U\frac{\left[(\sigma_p+\Delta\sigma)^2+\sigma_{int}^2\right]}{n+1} > V\frac{\left(\sigma_p^2+\sigma_{int}^2\right)}{n+1}\right) \\ = &\quad P\left(\frac{U}{V} > \frac{\sigma_p^2+\sigma_{int}^2}{(\sigma_p+\Delta\sigma)^2+\sigma_{int}^2}\right) \\ = &\quad 1 - F\left[\frac{\sigma_p^2+\sigma_{int}^2}{(\sigma_p+\Delta\sigma)^2+\sigma_{int}^2}\right] \end{aligned} \tag{A2}$$

where F is the F-distribution, with degrees of freedom n and n.

Also allowing a sensory threshold

This simple formula (Equation A2) cannot be used when we allow a sensory threshold, but note that if $f_X(x;n)$ and $F_X(x;n)$ are the PDF and CDF for a chi-square random variable X, with n degrees of freedom; then $f_X(x/a;n)/a$ and $F_X(x/a;n)$ will be the PDF and CDF for aX, as long as $a > 0$. Therefore, the CDF for N can be written as

$$F_N(x) = F_X\left[x(n+1) / \left(\sigma_p^2 + \sigma_{int}^2\right) n\right] \quad \text{(A3)}$$

and the PDF and CDF for S are

$$f_S(x) = \frac{f_X\left(x[n+1] / \left[(\sigma_p + \Delta\sigma)^2 + \sigma_{int}^2\right] n\right)(n+1)}{\left[(\sigma_p + \Delta\sigma)^2 + \sigma_{int}^2\right]} \quad \text{(A4)}$$

and

$$F_S(x) = F_X\left(x[n+1] / \left[(\sigma_p + \Delta\sigma)^2 + \sigma_{int}^2\right] n\right) \quad \text{(A5)}$$

Now consider what happens when there is a sensory threshold c, below which all sample variances are indistinguishable from zero. Either the sample variance from the first interval (the one with the larger variance) could be bigger than that from the second interval, or neither sample variance could exceed the threshold and the observer makes a lucky guess. Therefore, the expected response accuracy for 2AFC would be

$$\begin{aligned} P(C) = & \quad P(S \geq c, S > N) + \tfrac{1}{2} P(S < c, N < c) \\ = & \quad \int_c^\infty F_N(x) f_S(x)\, dx + \tfrac{1}{2} F_N(c) F_S(c) \end{aligned} \quad \text{(A6)}$$

Weber's Law

In this final section, we argue that 2AFC responses based on sample variance automatically produce Weber's Law, a consequence first noted by Green and Swets (1966). The only constraint is that the stimuli only vary in variance. That is, if the CDF of stimulus values $F_X(x)$, is such that

$$F_X(x) = F\left[x / \sqrt{varX}\right] \forall X \quad \text{(A7)}$$

then it can be shown that

$$F_{S_X^2}(x) = F_{S^2}[x / varX] \quad \text{(A8)}$$

where $F_{S_X^2}(x)$ is the CDF of S_X^2, the sample variance of X, and $F_{S^2}(x)$ is the CDF of S^2, a same-sized sample of $X / \sqrt{varX}$.

To obtain the expected response accuracy, we can set $y = x/\text{var } S$, and substitute into Equation A1:

$$P(C) = \int_0^\infty F_{S^2}\left(\frac{varS}{varN} y\right) f_{S^2}(y)\, dy \quad \text{(A9)}$$

Europe PMC Funders Author Manuscripts

Let us assume that the pedestal is sufficiently large so that we can forget about the internal noise and any sensory threshold (i.e. $\sigma_{\mathrm{p}}^2 \gg \sigma_{int}^2, c$). In that case,

$$P(C) = \int_0^\infty F_{S^2}\left[y\left(1+\frac{\Delta\sigma}{\sigma_{\mathrm{p}}}\right)^2\right] f_{S^2}(y)\,dy \quad \text{(A10)}$$

That is, the expected response accuracy is purely a function of $\Delta\sigma/\sigma_{\mathrm{p}}$. This is Weber's Law.

References

Barlow HB. The Ferrier Lecture, 1980. Critical limiting factors in the design of the eye and visual cortex. Proceedings of the Royal Society of London B: Biological Sciences. 1981; 212:1–34.

Brainard DH. The Psychophysics Toolbox. Spatial Vision. 1997; 10:433–436. [PubMed: 9176952]

Burr DC. Motion smear. Nature. 1980; 284:164–165. [PubMed: 7360241]

Burr DC. Temporal summation of moving images by the human visual system. Proceedings of the Royal Society of London B: Biological Sciences. 1981; 211:321–339.

Burr DC, Morgan MJ. Motion deblurring in human vision. Proceedings of the Royal Society B: Biological Sciences. 1997; 264:431–436.

Dakin SC. Orientation variance as a quantifier of structure in texture. Spatial Vision. 1999; 12:1–30. [PubMed: 10195386]

Dakin SC, Watt RJ. The computation of orientation statistics from visual texture. Vision Research. 1997; 37:3181–3192. [PubMed: 9463699]

Efron, B. The jackknife, the bootstrap and other resampling plans. Society for Industrial and Applied Mathematics; Philadelphia: 1982.

Foley JM. Human luminance pattern-vision mechanisms: Masking experiments require a new model. Journal of the Optical Society of America A, Optics, Image Science, and Vision. 1994; 11:1710–1719.

Foley JM, Legge GE. Contrast detection and near-threshold discrimination in human vision. Vision Research. 1981; 21:1041–1053. [PubMed: 7314485]

Georgeson, MA. From filters to features: Location, orientation, contrast and blur. In: Bock, GR.; Goode, J., editors. Higher-order processing in the visual system. Wiley; Chichester: 1994.

Green, DM.; Swets, JA. Signal detection theory and psychophysics. 1st ed. Wiley; New York: 1966.

Hoel, PG.; Port, SC.; Stone, CJ. Introduction to statistical theory. Houghton Mifflin; Boston: 1971.

Kingdom FA, Prins N, Hayes A. Mechanism independence for texture-modulation detection is consistent with a filter-rectify-filter mechanism. Visual Neuroscience. 2003; 20:65–76. [PubMed: 12699084]

Laming, D. Sensory analysis. Academic Press; 1986.

Legge GE, Foley JM. Contrast making in human vision. Journal of the Optical Society of America. 1980; 70:1458–1471. [PubMed: 7463185]

Mansouri B, Allen HA, Hess RF, Dakin SC, Ehrt O. Integration of orientation information in amblyopia. Vision Research. 2004; 44:2955–2969. [PubMed: 15380999]

Morgan, MJ. Hyperacuity. In: Regan, D., editor. Spatial vision. Macmillan; London: 1990. p. 87-113.

Morgan MJ, Benton S. Motion-deblurring in human vision. Nature. 1989; 340:385–386. [PubMed: 2755488]

Morgan MJ, McEwan W, Solomon J. The lingering effects of an artificial blind spot. PloS ONE. 2007; 2:e256. [PubMed: 17327917]

Motoyoshi I, Nishida S. Visual response saturation to orientation contrast in the perception of texture boundary. Journal of the Optical Society of America A, Optics, Image Science, and Vision. 2001; 18:2209–2219.

Nachmias J, Sansbury RV. Letter: Grating contrast: Discrimination may be better than detection. Vision Research. 1974; 14:1039–1042. [PubMed: 4432385]

Europe PMC Funders Author Manuscripts

Paakkonen A, Morgan MJ. The effects of motion blur on blur discrimination. Journal of the Optical Society of America A, Optics, Image Science, and Vision. 1993; 11:992–1002.

Parkes L, Lund J, Angelucci A, Solomon JA, Morgan M. Compulsory averaging of crowded orientation signals in human vision. Nature Neuroscience. 2001; 4:739–744.

Pelli DG. Uncertainty explains many aspects of visual contrast detection and discrimination. Journal of the Optical Society of America A, Optics and Image Science. 1985; 2:1508–1532.

Ross J, Speed H, Morgan M. The efffects of adaption and masking on incremental thresholds for contrast. Vision Research. 1993; 33:2050–2056.

Schwartz O, Sejnowski TJ, Dayan P. A Bayesian framework for tilt perception and confidence. Advances in Neural Information Processing Systems. 2006; 18

Solomon JA, Felisberti FM, Morgan MJ. Crowding and the tilt illusion: Toward a unified account. Journal of Vision. 2004; 4(6):9, 500–508. http://journalofvision.org/4/6/9/. doi:10.1167/4.6.9.

Solomon JA. Intrinsic uncertainty explains second responses. Spatial Vision. 2007; 20:45–60. [PubMed: 17357715]

Thompson P. The coding of velocity of movement in the human visual system. Vision Research. 1984; 24:41–45. [PubMed: 6695506]

Watson AB, Pelli DG. QUEST: A Bayesian adaptive psychometric method. Perception & Psychophysics. 1983; 33:113–120. [PubMed: 6844102]

Watt RJ, Morgan MJ. The recognition and representation of edge blur: Evidence for spatial primitives in human vision. Vision Research. 1983; 23:1465–1477. [PubMed: 6666047]

Wyszecki, G.; Stiles, WS. Color science. John Wiley and Sons; New York: 1967.

Europe PMC Funders Author Manuscripts

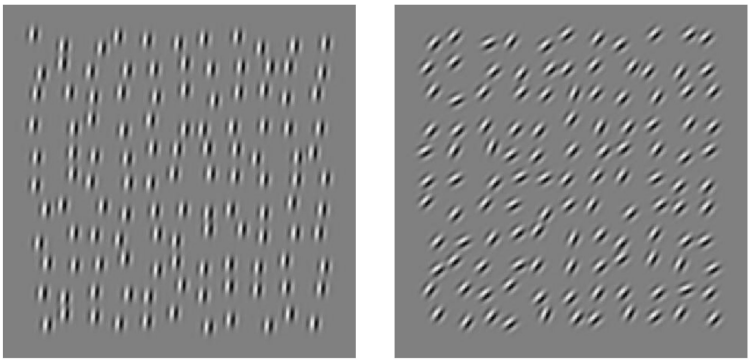

Figure 1.
Example of stimuli used in the variance discrimination experiment. The observer's task was to report which of the two images, which were presented successively, had the higher variability in orientation. In this case, there is zero variability in the image on the left; the image on the right was created using a Gaussian pdf with $\sigma = 8$ deg.

Europe PMC Funders Author Manuscripts

Europe PMC Funders Author Manuscripts

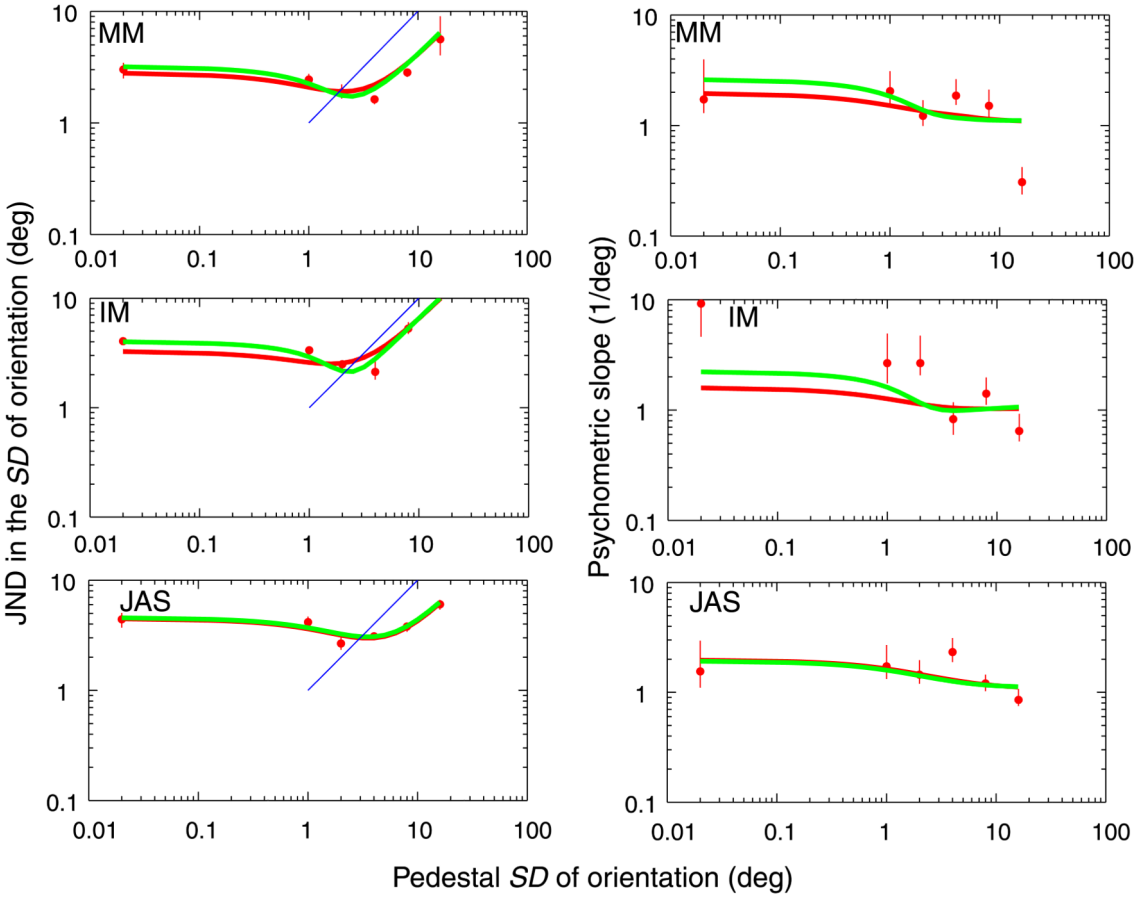

Figure 2.

The panels on the left hand side of the figure show just-noticeable differences in orientation variability between two patterns (vertical axis) for 3 observers (MM top panel; IM Middle panel; JAS bottom panel) as a function of the variability of the less-variable pattern (Pedestal, *x* axis). The data points (circles) show 82% correct values from best-fit Weibull functions, with 95% confidence limits (vertical bars). The red curves show the best fit to all the data of the ideal observer model described in the Appendix A; the green show the same model supplemented with a threshold (see also the Appendix A). The blue diagonal line has a unit slope for reference. The panels on the right hand side of the figure show the slopes of the best-fitting Weibull functions to the human (circles) and model (smooth curves) performances. The leftmost point in each graph refers to the Pedestal = 0 condition, moved to a small positive value to accommodate it on the logarithmic scale.

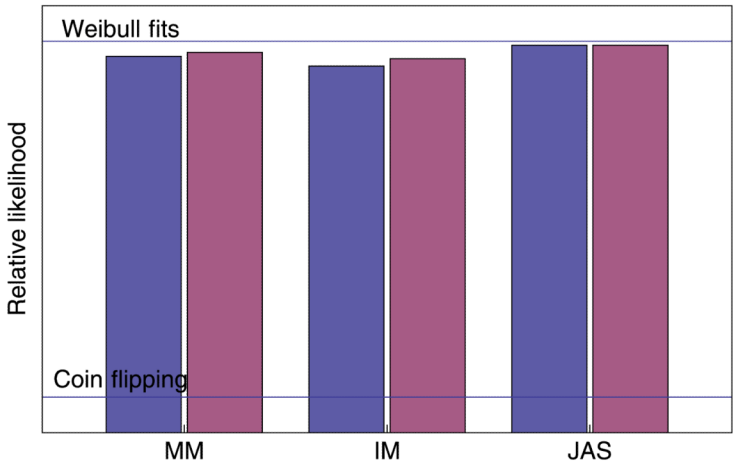

Figure 3.

The bars in the figure show relative likelihoods (different absolute scales of log likelihood for each observer) for the signal-detection model of variance discrimination (pink bars) and for the same model supplemented by a threshold (blue bars). The labeled horizontal lines show the likelihoods of a coin-flipping model and of separate Weibull fits to the data at each pedestal value. For further explanation, see the text.

Europe PMC Funders Author Manuscripts

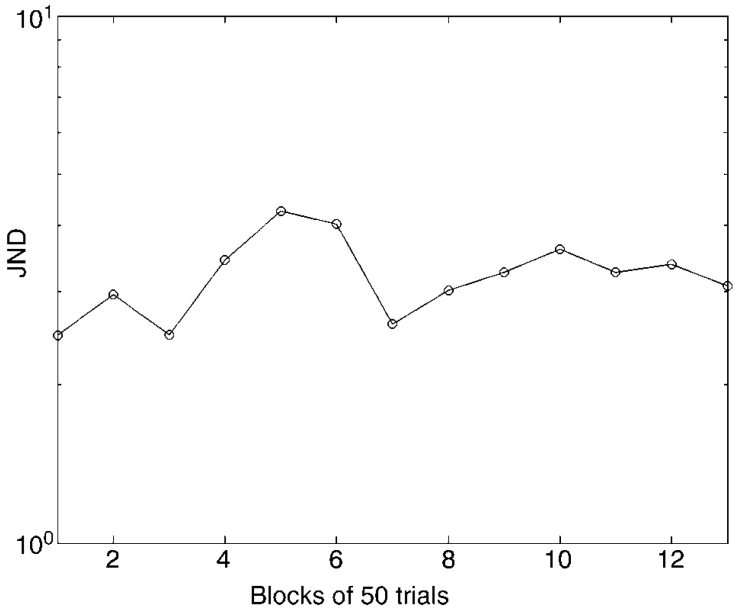

Figure 4.

Results of an experiment with a single observer (MM) to see whether extensive experience with variance detection could improve performance. The first six points show performance in the six blocks when the pedestals were interleaved (Figure 2). The last seven points show blocks when the zero pedestal condition was presented in isolation. There was no evidence for learning.

Europe PMC Funders Author Manuscripts

Table 1

Best fitting values for intrinsic noise σ_{int}, number samples $n + 1$, sensory thresholds c, and log-likelihoods (ln L) for three observers (MM, IM, and JAS). The models are described in the Appendix A. The asterisks show when the threshold model is a significantly better fit ($p < .01$) than the nonthreshold model.

	σ_{int}	$n + 1$	c	ln L
MM no thresh	2.87	9	–	−647.10
MM + thresh	2.23	8	3.16	−642.11**
IM no thresh	2.49	5	–	−504.83
IM + thresh	0.98	4	2.86	−495.91**
JAS no thresh	4.80	10	–	−1010.6
JAS + thresh	4.82	9	1.04	−1010.6 (NS)